Title

EFMouse: a Matlab toolbox to model stimulation-induced electric fields in the mouse brain

Authors

Ruben Sanchez-Romero[1], Sibel Akyuz[1], Bart Krekelberg[1]

[1] Center for Molecular and Behavioral Neuroscience, Rutgers University, Newark, NJ, 07102, USA

* Corresponding author: ruben.saro@rutgers.edu (R. Sanchez-Romero)

Format: Original research software article

Highlights

- EFMouse is a novel, open-source, Matlab-based electric field simulator for the mouse brain.
- EFMouse quantifies induced field focality and homogeneity in regions of the Allen Mouse Brain Atlas.
- Focal and strong stimulation can be produced with two- or five-electrode montages.
- A high-density montage with a lumbar return generates fields perpendicular to the cortical surface.

Abstract

Compared to the rapidly growing literature on transcranial electrical stimulation (tES) in humans, research into the mechanisms underlying neuromodulation by tES using in-vivo animal models is growing but still relatively rare. Such research, however, is key to overcome experimental limitations in humans and essential to build a detailed understanding of the in-vivo consequences of tES that can ultimately lead to development of targeted and effective therapeutic applications of non-invasive brain stimulation. The sheer difference in scale and geometry between animal models and the human brain contributes to the complexity of designing and interpreting animal studies. Here, we introduce EFMouse, a toolbox that extends previous approaches to model intracranial electric fields and is optimized to generate predictions that can be tested with in-vivo intracranial recordings in mice. Although the EFMouse toolbox has general applicability and could be used to predict intracranial fields for any electrical stimulation study using mice, we illustrate its usage by comparing fields in a tES high-density multi-electrode montage with a more traditional two-electrode montage. Our simulations show that both montages can produce strong focal homogeneous electric fields in targeted areas. However, the high-density montage produces a field that is more perpendicular to the visual cortical surface, which is expected to result in larger changes in neuronal excitability. The EFMouse toolbox is publicly available at https://github.com/klabhub/EFMouse.

Keywords: electrical stimulation; electric field modeling; mouse models; high-definition stimulation.

Author summary
Transcranial electrical stimulation offers new opportunities for studying brain activity and developing potential therapies. While this technique has been extensively applied in humans, our understanding of its neural consequences is still limited. Animal models offer an opportunity to bridge this gap. However, due to differences in size and brain structure, designing and interpreting electrical stimulation protocols for animal models is challenging. To address this, we developed EFMouse, an open-source computational toolbox that predicts intracranial electrical fields in the mouse brain during stimulation. This toolbox allows researchers to design experiments by simulating electrode arrangements and quantifying properties of the predicted electric field in specific brain regions. By doing so, EFMouse can guide the optimization of stimulation techniques to achieve targeted and reproducible effects. We illustrate its use by comparing a two-electrode and a five-electrode arrangement, in terms of the strength, focality, and direction of their induced electric field. By making EFMouse publicly available, we hope to advance fundamental neuroscience research and the development of future clinical applications.

Data/code availability statement: All code and data to reproduce our analyses are available at the EFMouse toolbox repository https://github.com/klabhub/EFMouse. EFMouse was implemented in Matlab2023a. For the Allen atlas analysis, FSL 6.7.0 onwards is required (https://fsl.fmrib.ox.ac.uk/fsl/). EFMouse toolbox repository DOI https://doi.org/10.5281/zenodo.14777233 points to the latest version release.

Declaration of interests: The authors have no conflicts of interest to declare.

Author statement:
Ruben Sanchez-Romero: Conceptualization, Methodology, Software, Formal Analysis, Writing-original draft, Writing-review & editing, Visualization.
Sibel Akyuz: Conceptualization, Methodology, Writing-review & editing.
Bart Krekelberg: Conceptualization, Methodology, Software, Writing-review & editing, Supervision, Resources, Funding acquisition.

Financial Disclosure: Research reported in this publication was supported by the National Institute Of Neurological Disorders And Stroke (https://www.ninds.nih.gov/) and the National Institute on Drug Abuse (https://nida.nih.gov/) of the National Institutes of Health under Award Number R01NS120289, for B.K. The content is solely the responsibility of the authors and does not necessarily represent the official views of the National Institutes of Health. The funding institution did not play any role in the study design, data collection and analysis, decision to publish, or preparation of the manuscript.

Introduction

Understanding intracranial current flow is an important aspect of harnessing the potential of transcranial current stimulation. In-vivo intracranial measurements provide the most direct assessment of intracranial fields caused by tES. Opitz et al., (2016, 2018) and Huang et al., (2017) provide such measurements of electric field magnitudes in humans. While important, such studies with human volunteers are limited because recording electrodes are placed based on clinical considerations and not to test the properties of induced electric fields. These limitations are partially addressed by translational work in animal models (Asan et al., 2019; Kar et al., 2017; Opitz et al., 2016) and human cadavers (Vöröslakos et al., 2018; Violante et al., 2023), although these come with a different set of caveats (Opitz et al., 2017). Reviews by Beliaeva et al., (2021) and Jackson et al., (2016) provide a list of considerations to better translate electrical stimulation experiments in rodents and non-human primates to humans, for example, differences in brain geometry that determine the flow of electric current, orientation of targeted neuronal columns and placement of stimulation electrodes, organization of functional networks related to targeted behavior, and the need to adjust parameters, such as the injected current, to achieve field magnitudes that could realistically be achieved in human applications.

Given the technical challenges of intracranial field recordings, electric field models provide an important complementary approach to investigating various conditions of interest. For instance, Alekseichuk et al. (2019) used high-resolution anatomical mesh models to compare electric fields across mouse, monkey, and human brains, and Bernabei et al. (2014) used the same anatomical mouse mesh to simulate a montage with one electrode clipped in each ear. These studies primarily reported results at the whole-brain level—emphasizing general similarities and differences between species. Here, we build on these approaches by developing a mouse electric field model (EFMouse) specifically for experiments in which the neural consequences of stimulation are measured invasively, for example, with intracranial recording electrodes or two-photon imaging (e.g., Dadarlat et al., (2024)). This required several refinements that were not available in other open-source electric field modeling software packages optimized for non-invasive stimulation of human brains (SimNIBS (Thielscher et al., 2015) and ROAST (Huang et al., 2019)). 1) We modeled the skin removal and the craniotomies that are necessary to probe intracranial responses. For example, in EFMouse, users can model a cranial recording window and analyze the predicted electric field in the underlying cortical region. This feature increases the validity of the model predictions by considering surgery-induced tissue inhomogeneities affecting the current flow. 2) We developed an approach that allows the stimulation electrodes to be placed in any tissue or region of the animal's body. For instance, users can model stimulation electrodes positioned intracranially, on the skin or bone of the mouse head or on other commonly used body parts, such as the lumbar region, submandibular area, or neck. 3) We created tools to quantify field properties in arbitrary regions of interest defined by stereotaxic coordinates or in identified regions of the Allen Mouse Brain Atlas. Users can quantify the electric field on a whole-brain basis, compare fields in target (e.g., under the cranial window) and off-target regions of interest, or use the Allen atlas to analyze the field properties across well-defined functional areas. These novel functionalities bring us closer to a model that informs questions about target and off-target stimulation, enables the comparison of the relative benefits of different montages, and ultimately predicts specific (neural or behavioral) outcomes in an experiment.

In this paper, we present the considerations and technical solutions that led to EFMouse (Design and Implementation) and then illustrate its use by asking a series of questions about a planned experiment in which electrical stimulation is used to target the mouse visual cortex and the neural consequences are recorded using two-photon imaging (Results). Researchers can adapt EFMouse to their questions following the Matlab tutorials in the project repository (https://github.com/klabhub/EFMouse).

Design and Implementation

Mouse mesh

We use the mesh mouse model published by Alekseichuk et al. (2019), based on images provided by the Digimouse project (Dogdas et al., 2007). In short, the mesh corresponds to one 28-gram normal nude male mouse for which post-mortem isotropic 0.1mm voxel images were acquired (CT, PET, and cryosection). The high-resolution mesh provided by Alekseichuk et al. consists of approximately 1M nodes and 5.7M tetrahedra and segments the mouse's whole body into five broad structures with corresponding conductivity values: gray matter (0.275 Siemens per meter, S/m), CSF (1.654 S/m), bone (0.01 S/m), soft tissue (0.465 S/m) and eyeballs (0.5 S/m). We changed the mesh's orientation to left to right (x-axis), posterior to anterior (y-axis), and inferior to superior (z-axis) to match the conventions of the Paxinos atlas (Paxinos and Franklin, 2019).

Craniotomy

Measuring neural consequences of stimulation at the single neuron level requires an invasive approach and, therefore, a craniotomy. Modeling this included two components. First, to model the removal of the skin, we set the conductivity of the skin tetrahedra above the craniotomy to that of air (2.5e-14 S/m, value taken from ROAST (Huang et al., 2019) (https://github.com/andypotatohy/roast/)). Second, we assumed that cerebral spinal fluid (CSF) would fill the volume of the removed skull. To model this, we set the conductivity of the tetrahedra corresponding to the removed skull volume to that of CSF.

Electrode placement

Following the same approach as for the craniotomy, we modeled electrodes by changing the conductivity values of existing elements of the tetrahedral mesh to a highly conductive 5.9e7 S/m (value taken from ROAST). In our experiments (see Results), we modeled circular electrodes of 1 mm diameter and 0.85 mm depth placed in the skin tetrahedra. For the 4x1 montage, we placed four anodes in anterior, posterior, lateral, and medial positions surrounding the craniotomy and one cathode in the lumbar area of the mouse (**Figure 1A**). We selected 0.2 mA total current based on the experiments of Asan et al. (2020) and Dockery et al. (2011). We distributed this current across the four anodes (+0.5 mA each) while returning all current through the single cathode (-0.2 mA). For the 1x1 montage, we placed an anode anterior to the craniotomy and a cathode posterior (**Figure 1B**). In the 1x1 montage, the anode received +0.2 mA, and the cathode returned -0.2 mA (**Figure 1B**). These parameters were specifically selected for our experiments; however, researchers can modify them to suit their experimental conditions.

Guiding placement

The mesh's anatomical resolution does not provide detailed landmarks. To improve the placement of instrumentation (e.g., the craniotomy and the electrodes), we manually coregistered the Digimouse's volumetric NIfTI files with the visual areas defined in the Allen atlas (see **Figure 4** for a volume slice example). EFMouse provides a function to map from volumetric coordinates to mesh coordinates. (Digimouse and Allen atlas NIfTI files are provided in the repository.)

Electric field modeling

The finite element method (FEM) solution for the electric field problem described by the mouse, craniotomy, electrodes, conductivities, and injected currents, is based on the ROAST implementation but adjusted to the

specifics of our mouse model. In contrast to human-optimized tES simulators, our electrodes do not use conductive gel but are inserted directly into the mouse tissue (e.g., skin or bone); this is reflected in the definition of the electrode boundary conditions. We solved the FEM electrostatic problem using the open-access solver GetDP (Dular et al., 1998) (https://getdp.info/), keeping the ROAST default parameters. The solution results in a voltage (V), electric field components in x,y, and z directions (V/m), and an electric field magnitude (V/m) at each node in the mesh.

Relative focality

Extending the definition of focality used by Fernandes et al. (2024), we define a highly focal montage as one in which few areas outside the target area have *eMag* values as high as the ones observed in the target area. Such a montage produces a strong electric field concentrated in the target area. Low focality indicates the opposite: many reference areas have *eMag* values as high as the target area—a montage with more diffuse effects. To capture this, we defined relative focality as: one minus the fraction of nodes in a *reference area* with an electric field magnitude (*eMag*) greater than 75% of the *target area's* 99.9th percentile of its *eMag* distribution. Our measure of relative focality ranges from zero to one. Values close to zero indicate low relative focality, values close to one indicate high relative focality.

Direction homogeneity

In-vitro recordings show the importance of the direction of the induced field relative to the orientation of the major axis of the neurons (Bikson et al., 2004; Lafon et al., 2017). Based on such results, a field with a small magnitude aligned homogeneously with the neurons could have a bigger influence than a misaligned field with a large magnitude. We define direction homogeneity as the magnitude of the mean of the normalized components across all nodes in a given region.

Direction homogeneity is thus computed as $\mathrm{sqrt}(\mathrm{mean}(eX_n)^2 + \mathrm{mean}(eY_n)^2 + \mathrm{mean}(eZ_n)^2)$, where $eX_n = eX/eMag$ is the normalized field component in the x direction for each mesh node, equivalently for eY_n and eZ_n. We use normalized components to consider only the direction of the field and not its magnitude. Also, using normalized components, direction homogeneity ranges from 0 to 1, with larger values indicating more homogeneity and thus electric field components with a more uniform direction. (Consider an extreme example where half of the nodes point to the positive-x direction and the other half to the negative-x direction; the field direction homogeneity will be zero.) In the Results section, we report direction homogeneity and mean normalized x, y, and z components.

Implementation

The toolbox was implemented using an object-oriented approach in Matlab R2023a. The code is documented extensively, includes tutorials matching the simulations presented in this paper, and is available at https://github.com/klabhub/EFMouse. All the modeling parameters in EFMouse are configurable, allowing users to adjust them at will. We provide active support to users via the repository Issues section. For the Allen atlas analysis, FSL 6.7.0 onwards is required (https://fsl.fmrib.ox.ac.uk/fsl/).

Results

We developed a Matlab toolbox (EFMouse) to simulate intracranial fields in the mouse brain induced by current stimulation. The GitHub repository (https://github.com/klabhub/EFMouse) contains tutorials and tools that allow researchers to ask specific questions. Here, we illustrate its use by asking a series of questions from ongoing

experiments investigating the neural consequences of transcranial direct current stimulation (tDCS) using two-photon imaging. In these experiments, the goal was to target the left visual cortex of the mouse while recording neural activity using two-photon microscopy. (For similar experimental setups, see Monai et al., (2016), Michelson et al. (2019), and Dadarlat et al. (2024).)

Our first question was whether a high-density montage provides an advantage over a traditional two-electrode montage. The reported behavioral effects of tES with high-definition montages suggest that such electrode arrangements offer a promising approach for developing effective stimulation protocols. However, the properties of the resulting fields and their neural consequences remain less well understood. (To our knowledge, no experiments have been reported in mice using high-definition montages and intracranial recordings.) High-definition montages aim to increase the focality of the induced electric field in targeted areas and generally use a center-surround arrangement with varying numbers of electrodes (Dmochowski et al., 2011; Edwards et al., 2013). Studies using high-definition montages for transcranial alternating current stimulation (tACS) or tDCS have reported significant behavioral effects, for example, in motion perception (Helfrich et al., 2014); visuospatial working memory and mental rotation (Zhang et al., 2022); feedback guided learning (Reinhart, 2017); and working memory in older adults (Reinhart and Nguyen, 2019). These findings suggest that the focality of the high-definition montages plays a role in the effectiveness of transcranial stimulation. Direct behavioral evidence to support such a claim can be found in a small number of studies that directly compare high-definition vs. conventional montages. For instance, Gözenman and Berryhill (2016) show a statistical interaction between montage and working memory conditions and speculate that the difference in behavioral effects could be explained in terms of focality (affecting a region of interest) or diffusivity (affecting a large-scale network) of the induced electric field. (See also Hogeveen et al., (2016) and Masina et al., (2021).)

To explore this question in a mouse model, we simulated a high-density 4x1 montage (**Figure 1A**) and a conventional 1x1 montage (**Figure 1B**), both with stimulation electrodes inserted into the skin (red) and a craniotomy representing the removal of skin (green) and bone (yellow) (Design and Implementation).

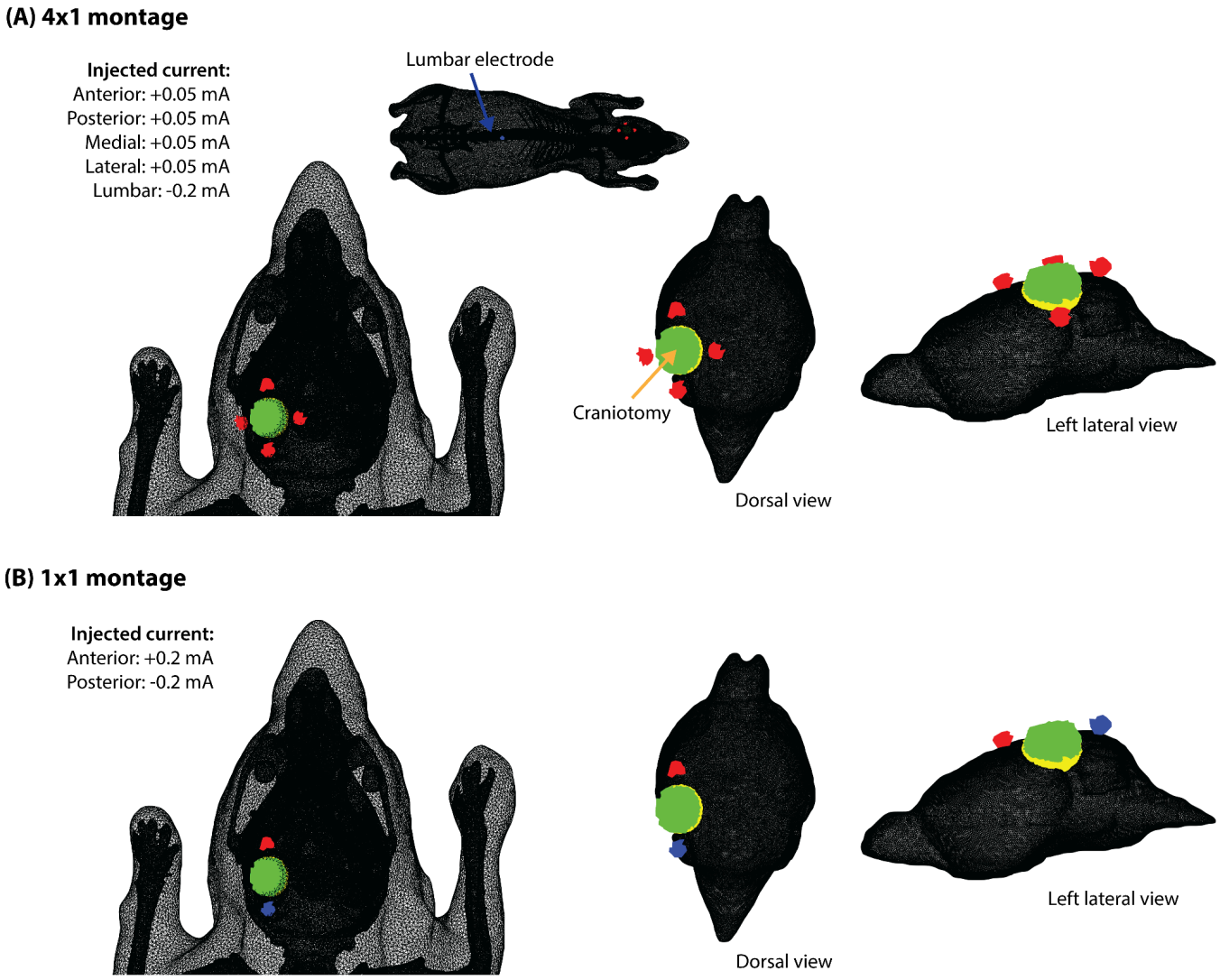

Figure 1. Craniotomy and electric stimulation montage. Visualization in mesh space for (A) 4x1 montage and (B) 1x1 montage. The montage is represented relative to the mouse skin and bone (left panels) and relative to the mouse brain (right panels). Skin removal is depicted in green, underlying bone removal is in yellow, anodes are in red, and cathodes are in blue.

Whole brain electric field

We start with an analysis of the predicted field at the whole brain level (labeled in the Digimouse/Alekseichuk mesh as “gray matter”; it contains olfactory bulbs, cortex, subcortex, cerebellum, and the brainstem) to visualize the general spatial patterns of the field across the brain (**Figure 2**). Visual inspection of **Figure 2** suggests that both montages target the left visual cortex: the area surrounding craniotomy and electrodes has a higher field magnitude than the contralateral right area. This overall view, however, glosses over some potentially important differences.

Table 1 shows that both montages achieve a similar field magnitude (mean and median). However, the 4x1 montage has a large dorsal to ventral component (the negative component in the z-direction, mean eZ = -1.66 V/m) and a lateral to medial component (the positive component in the x direction, mean eX = 1.27 V/m), consistent with the position of the lumbar return electrode (see **Figures 1A**, **2A**). In contrast, the 1x1 montage

primarily generates a tangential field (anterior-to-posterior, negative component in the y direction, mean *eY* = -1.67 V/m), consistent with the position of the return electrode (see **Figures 1B**, **2B**). These differences are also reflected in the direction homogeneity measure (Design and Implementation), which is 0.83 for the 4x1 montage with mean normalized components (0.51, -0.16, -0.63), indicating more uniform components in the positive-x and negative-z directions. By contrast, the 1x1 montage has a direction homogeneity of 0.72 with (0.31, -0.59, -0.26), indicating a more uniform component in the negative-y direction. (Note that we report results here only for the mouse *brain*. However, EFMouse can also produce electric field summary statistics for the other mesh tissues/elements, including soft tissue, bone, CSF, eyeballs, craniotomy, and electrodes. See the tutorial Matlab notebooks in the repository).

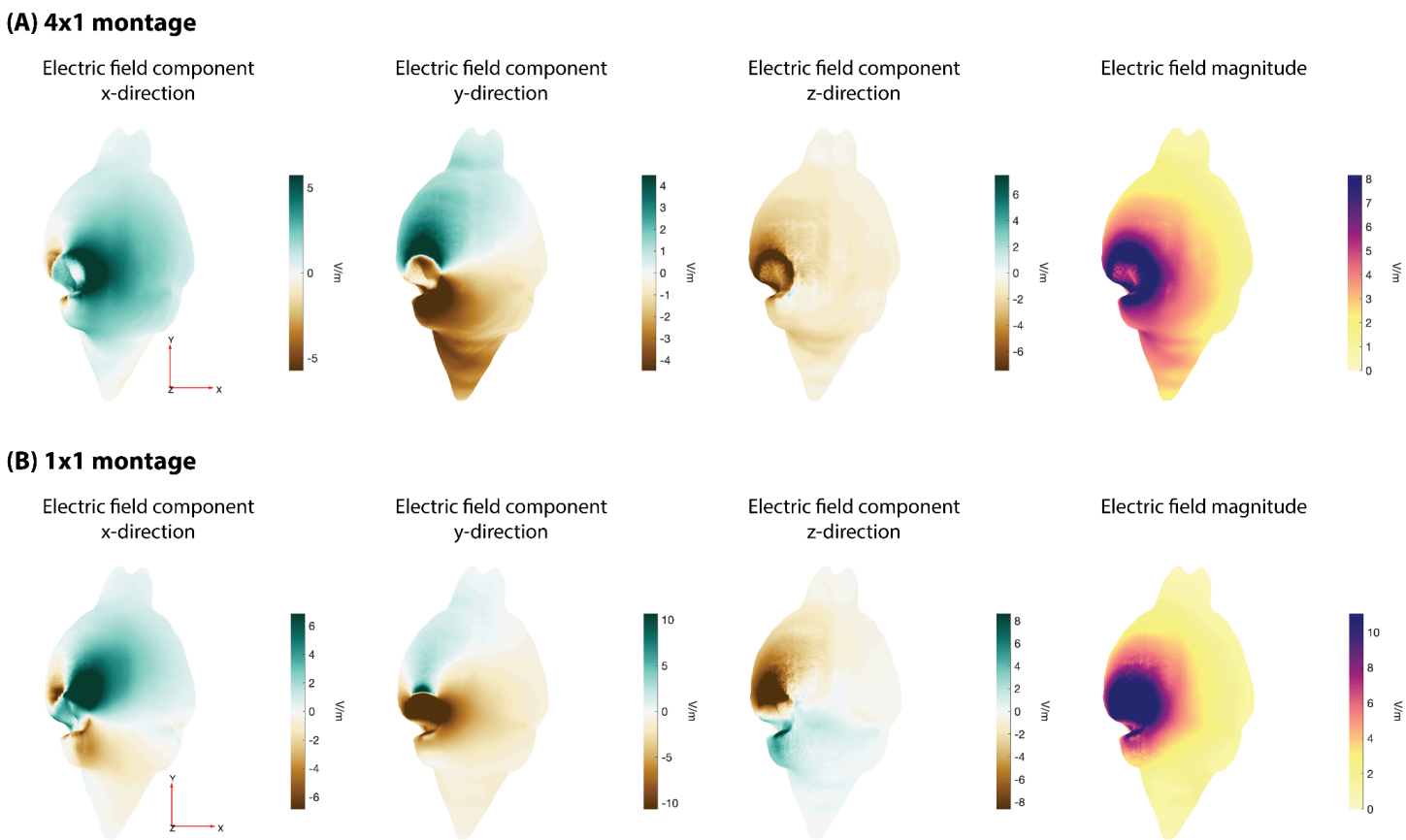

Figure 2. Predicted electric field (V/m) in the whole Digimouse brain. Visualization in mesh space. Results for (A) 4x1 and (B) 1x1 montages. Field magnitudes are capped at the 98th percentile to remove outliers from this visualization.

Table 1. Summary statistics for the predicted electric field (V/m) in the Digimouse brain. Results for the x, y, and z direction field components (*eX*, *eY,* and *eZ*) and the field magnitude (*eMag*) for the 4x1 and 1x1 montages.

Whole brain											
	4x1 montage						**1x1 montage**				
	mean	**median**	**std**	**min**	**max**		**mean**	**median**	**std**	**min**	**max**
eX	1.27	0.99	1.15	-5.42	14.53	***eX***	0.79	0.68	1.68	-11.72	26.46
eY	-0.55	-0.31	1.55	-12.78	12.11	***eY***	-1.67	-1.36	2.27	-31.97	19.52
eZ	-1.66	-1.27	1.38	-16.31	2.56	***eZ***	-0.75	-0.40	2.12	-40.61	12.77
eMag	2.64	2.15	1.83	0.21	18.90	***eMag***	2.83	1.99	2.91	0.16	46.88

Region of Interest under the craniotomy

In our planned experiments we will measure neural response properties in the visual cortex below the craniotomy, therefore we are particularly interested in the properties of the predicted electric field in this area. We report results for a box-shaped region of interest (ROI) under the left hemisphere craniotomy (with dimensions x = 1.45 mm, y = 1.24 mm, z = 1 mm) (**Figure 3A**), and for comparison an analogous ROI in the right hemisphere with the same dimensions (**Figure 3B**). Results in **Table 2A** show that for the ROI under the craniotomy, (a) the 1x1 montage produces a stronger mean magnitude; (b) the 4x1 field generates a strong dorsal-to-ventral field (mean eZ = -7.34 V/m), while the field produced by the 1x1 montage is primarily in the tangential anterior-to-posterior y direction, mean eY = -8.54 V/m). Results in **Table 2B** for the comparison ROI in right visual cortex show that (a) both montages produce weaker fields, and (b) consistent with the whole brain results (**Table 1**), the 4x1 field has preferred negative-z and positive-x directions, while, the 1x1 file has a preferred negative-y direction.

For the 4x1 montage, the ROI under the left craniotomy has a direction homogeneity of 0.99 with mean normalized components (0.38, -0.06, -0.91), while the 1x1 montage has a direction homogeneity of 0.94 with components (0.30, -0.89, 0.02). For the comparison ROI in the right visual cortex, the 4x1 montage has a direction homogeneity of 0.99 with (0.69, -0.42, -0.58), and the 1x1 montage reports 0.98 with (0.11, -0.97, -0.10).

To compute relative focality, we consider the ROI under the craniotomy as the *target area* and the rest of the brain as the *reference area* (Design and Implementation), similarly for the comparison ROI. For the ROI under the craniotomy, the 4x1 montage relative focality was 0.989. For the 1x1 montage, it was 0.988. (The reference area comprises 161,805 brain mesh nodes). In this analysis, both montages are highly focal, with only ~1% of the brain outside the target area receiving a field that was similar to that inside the target area (Design and Implementation). For the comparison ROI in the right visual cortex, the 4x1 montage relative focality was 0.356, and for the 1x1 montage it was 0.428. (The reference area comprises 161,865 brain mesh nodes).

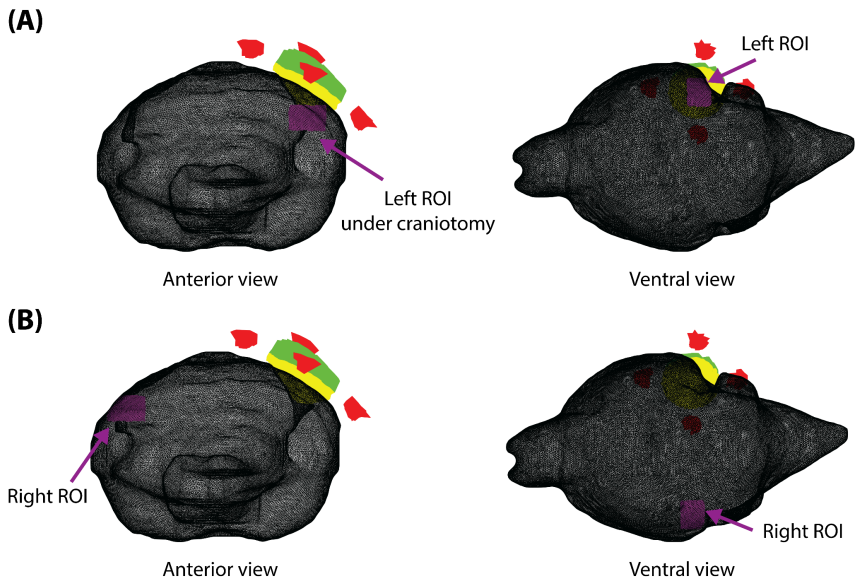

Figure 3. Two box-shaped regions of interest (ROIs) in the mouse visual cortex. Visualization in mesh space. A target ROI is located in the left visual cortex under the craniotomy. The comparison ROI with analogous dimensions is in the contralateral right visual cortex. Electrodes and craniotomy for the 4x1 montage only. ROIs are depicted in magenta. (The same ROIs were used for the 1x1 montage.)

Table 2. Summary statistics for the predicted electric field (V/m) for two box-shaped regions of interest (ROIs) in the mouse visual cortex. Results for (A) ROI under craniotomy in the left visual cortex and (B) analogous ROI in the contralateral right visual cortex. Results for the x, y, and z direction field components (*eX*, *eY,* and *eZ*) and the field magnitude (*eMag*) for the 4x1 and 1x1 montages.

(A) ROI under craniotomy in left visual cortex

	4x1 montage						1x1 montage				
	mean	**median**	**std**	**min**	**max**		**mean**	**median**	**std**	**min**	**max**
eX	3.04	2.84	1.14	0.48	8.57	***eX***	2.51	2.57	1.16	-1.49	5.42
eY	-0.47	-0.36	0.95	-4.23	1.62	***eY***	-8.54	-7.98	3.06	-16.53	-2.77
eZ	-7.34	-7.32	1.29	-10.48	-3.54	***eZ***	-0.06	0.44	2.63	-9.18	4.86
eMag	8.09	8.01	1.36	4.45	12.90	***eMag***	9.42	8.67	2.83	5.32	18.62

(B) ROI in right visual cortex

	4x1 montage						1x1 montage				
	mean	**median**	**std**	**min**	**max**		**mean**	**median**	**std**	**min**	**max**
eX	1.28	1.29	0.21	0.71	1.73	***eX***	0.20	0.28	0.29	-0.64	0.72
eY	-0.77	-0.72	0.14	-1.19	-0.53	***eY***	-1.66	-1.62	0.28	-2.43	-1.04
eZ	-1.06	-1.06	0.11	-1.32	-0.74	***eZ***	-0.15	-0.15	0.11	-0.46	0.18
eMag	1.84	1.83	0.20	1.36	2.29	***eMag***	1.70	1.68	0.28	1.11	2.43

Allen atlas analysis

The ROI-based analysis above disregards anatomical and functional boundaries. Experimental questions, however, are more often formulated with respect to functionally meaningful regions of interest. EFMouse can quantify electric field properties using terms defined in the Allen Mouse Brain Atlas to address this. For instance, we computed field measures for the “visual areas” defined in the Allen atlas (**Figure 4**). Results in

Table 3A for the left visual cortex are consistent with (and complement) the ROI results from **Table 2A**: (a) the 1x1 montage produces a stronger field than the 4x1; (b) the 4x1 field has preferred negative-z and positive-x directions, while the 1x1 has a strong preference for the negative-y direction. In line with results from **Table 2B**, **Table 3B** shows that for the comparison areas in the right visual cortex, both montages produce weaker fields with similar magnitude that differ in their preferred directions, with the 4x1 field preferring the negative-z and positive-x directions, and the 1x1 field the negative-y direction.

For the areas defined as the left visual cortex in the Allen atlas, the 4x1 montage results in a direction homogeneity of 0.93 with mean normalized components (0.56, -0.05, -0.74), and the 1x1 montage results in a direction homogeneity of 0.88 with (0.34, -0.79, -0.18). For the comparison areas labeled right visual cortex, the 4x1 montage has a direction homogeneity of 0.99 with (0.78, -0.36, -0.48), and the 1x1 montage has 0.98 with (0.24, -0.95, -0.002).

To compute relative focality, we consider the left visual areas of the Allen atlas as the *target area* and the whole Allen atlas "isocortex" (excluding the left visual areas) as the *reference area*. Similarly for the comparison right visual areas. For the left visual cortex, the 4x1 montage relative focality was 0.998; for the 1x1 montage it was 0.999. (The isocortex reference area comprises 92,410 voxels). For the comparison areas of right visual cortex, the 4x1 montage relative focality was 0.621; for the 1x1 montage, it was 0.518. (The isocortex reference area comprises 92,457 voxels).

Table 3. Summary statistics for the predicted electric field (V/m) for the Allen Mouse Brain Atlas visual cortex. Results for (A) left visual cortex in the Allen atlas and (B) right visual cortex in the Allen atlas. Results for the x, y, and z direction field components (*eX*, *eY,* and *eZ*) and the field magnitude (*eMag*) for the 4x1 and 1x1 montages. (Rounding may show some values as zero.)

(A) Allen atlas left visual cortex

	4x1 montage						1x1 montage				
	mean	**median**	**std**	**min**	**max**		**mean**	**median**	**std**	**min**	**max**
eX	4.85	4.94	2.52	-2.19	12.86	***eX***	4.78	3.86	4.68	-5.48	23.52
eY	-0.41	-0.24	2.10	-10.01	7.31	***eY***	-10.72	-10.35	5.22	-28.13	3.35
eZ	-6.38	-6.75	2.53	-13.50	0.00	***eZ***	-3.42	-2.16	5.64	-31.19	10.11
eMag	8.58	8.77	2.87	0.00	16.27	***eMag***	13.91	12.97	6.13	0.01	36.79

(B) Allen atlas right visual cortex

	4x1 montage						1x1 montage				
	mean	**median**	**std**	**min**	**max**		**mean**	**median**	**std**	**min**	**max**
eX	1.71	1.84	0.77	0.00	3.04	***eX***	0.52	0.37	0.48	-0.60	2.28
eY	-0.76	-0.82	0.42	-1.65	0.14	***eY***	-1.95	-2.14	0.84	-3.50	0.00
eZ	-1.04	-1.12	0.46	-1.77	0.00	***eZ***	0.00	-0.06	0.27	-0.76	0.81
eMag	2.17	2.37	0.93	0.00	3.55	***eMag***	2.07	2.24	0.90	0.00	3.54

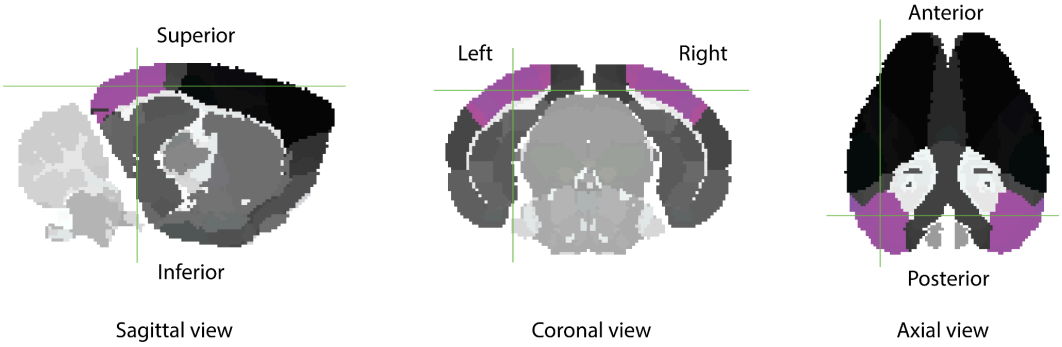

Figure 4. Allen Mouse Brain Atlas visual cortex. The areas labeled “Visual areas” in the Allen atlas are depicted here in magenta. The predicted electric field is analyzed separately for the left and right visual cortex (Table 3). (Allen atlas registered to Digimouse volumetric space. Representative slice at voxel (28,85,65) in the Allen atlas NIfTI file provided in the EFMouse repository. Image generated with FSLeyes.)

Availability and Future Directions

We developed a finite element model of the mouse brain to simulate and analyze electric fields produced by current stimulation. While the model has general applicability, we illustrate its use here by comparing the relative merits of a high-definition 4x1 montage and a traditional 1x1 montage, in a planned study investigating the neural consequences of tDCS in mouse visual cortex. We discuss the outcomes and limitations of this specific analysis, as well as some of the limitations and future directions for the EFMouse model.

At the coarse level of electric field magnitude (**Figure 2**, rightmost panels), the fields produced by the 4x1 and 1x1 montages look similar. While such brain surface maps are a common representation of applied fields in studies using tES, our analysis suggests they are lacking in some important aspects. First, quantifying target and off-target or control regions (whether defined using coordinate-based ROIs or regions in an atlas) helps understand the specificity of the applied stimulation. Second, this quantification should include some measure of focality that compares target and off-target areas. Third, we found that the 4x1 montage produced a predominantly radial field (aligned with the principal axis of most neurons in the mouse visual cortical surface). In contrast, the 1x1 montage generated a largely tangential field. Because in-vitro recordings show that neural outcomes depend on the alignment of the field with the stimulated neurons, quantifying this alignment could help to interpret and compare tES outcomes. These considerations apply equally or potentially even more forcefully to the human brain because its complex geometry and the extensive intersubject variability are expected to generate more inhomogeneous distributions of the magnitude and orientation of tES-induced fields.

EFMouse builds on previous work modeling current flow in the brain. We borrowed the mouse anatomical model from Alekseichuk et al. (2019) and the Digimouse project (Dogdas et al., 2007) and the general workflow in the Matlab implementation from ROAST (Huang et al., 2019). We added novel functionality to capture typical surgical approaches in the mouse (e.g., skin removal and cranial recording windows) and the placement of stimulation electrodes anywhere in or on the animal. These enhancements improve the model’s validity for experiments that include intracranial recording (e.g., Monai et al., (2016); Mishima et al., (2019)) and bone, epidural, or intracranial stimulation (e.g., Ozen et al. (2010); Dadarlat et al., (2024)). In addition, our software adds novel ways to report field predictions, including some refined measures of focality and direction homogeneity and mapping of simulation results to the Allen Mouse Brain Atlas.

One limitation of EFMouse is that it is based on the one nude male mouse from the Digimouse project (Dogdas et al., 2007). This strain differs from the more commonly used C57BL/6 strain, which is also used for the Allen atlas. Consequently, the coregistration of the Allen atlas to the Digimouse space will likely be imprecise at the level of the finest functional areas (e.g., cortical layers). If a high-resolution mesh for a C57BL/6 mouse becomes available, it could be incorporated into EFMouse, improving the neuroanatomical interpretation of the predicted electric fields.

The current version of EFMouse computes the orientation of the electric field in stereotaxic coordinates. This can be interpreted as radial or tangential orientations (relative to the cortical surface) for many cortical areas. However, this is more complex in cortical areas with strong curvature or in subcortical areas (which have not been segmented in the Digimouse mesh). Future work could address this by developing a more detailed segmentation of the whole mouse brain.

In contrast to human studies where anatomical variability can produce substantial differences in effects (Zanto et al., 2021; Preisig and Hervais-Adelman,2022; Hunold et al., 2023), the anatomical homogeneity of inbred mouse strains allows for highly generalizable simulation results across animals. However, when stimulation is combined with intracranial recordings, variability in surgical implants (e.g., location of craniotomies and stimulation electrodes) is a factor that may require individualized models.

In future work, we plan to compare these simulation results with neural data. Such direct comparisons are essential to validate the models and critically assess the assumptions underlying the practical or therapeutic application of tES. Ultimately, this should allow researchers to design targeted stimulation protocols and effective interventions in humans.

References

Alekseichuk, I., Mantell, K., Shirinpour, S., & Opitz, A. (2019). Comparative modeling of transcranial magnetic and electric stimulation in mouse, monkey, and human. *Neuroimage*, *194*, 136-148.

Asan, A. S., Gok, S., & Sahin, M. (2019). Electrical fields induced inside the rat brain with skin, skull, and dural placements of the current injection electrode. *PLoS One*, *14*(1), e0203727.

Asan, A. S., Lang, E. J., & Sahin, M. (2020). Entrainment of cerebellar purkinje cells with directional AC electric fields in anesthetized rats. *Brain stimulation*, *13*(6), 1548-1558.

Beliaeva, V., Savvateev, I., Zerbi, V., & Polania, R. (2021). Toward integrative approaches to study the causal role of neural oscillations via transcranial electrical stimulation. *Nature Communications*, *12*(1), 2243.

Bernabei, J. M., Lee, W. H., & Peterchev, A. V. (2014, August). Modeling transcranial electric stimulation in mouse: A high resolution finite element study. In *2014 36th Annual International Conference of the IEEE Engineering in Medicine and Biology Society* (pp. 406-409). IEEE.

Bikson, M., Inoue, M., Akiyama, H., Deans, J. K., Fox, J. E., Miyakawa, H., & Jefferys, J. G. (2004). Effects of uniform extracellular DC electric fields on excitability in rat hippocampal slices in vitro. *The Journal of physiology*, *557*(1), 175-190.

Dadarlat, M. C., Sun, Y. J., & Stryker, M. P. (2024). Activity-dependent recruitment of inhibition and excitation in the awake mammalian cortex during electrical stimulation. *Neuron*, *112*(5), 821-834.

Dmochowski, J. P., Datta, A., Bikson, M., Su, Y., & Parra, L. C. (2011). Optimized multi-electrode stimulation increases focality and intensity at target. *Journal of neural engineering*, *8*(4), 046011.

Dockery, C. A., Liebetanz, D., Birbaumer, N., Malinowska, M., & Wesierska, M. J. (2011). Cumulative benefits of frontal transcranial direct current stimulation on visuospatial working memory training and skill learning in rats. *Neurobiology of learning and memory*, *96*(3), 452-460.

Dogdas, B., Stout, D., Chatziioannou, A. F., & Leahy, R. M. (2007). Digimouse: a 3D whole body mouse atlas from CT and cryosection data. *Physics in Medicine & Biology*, *52*(3), 577.

Dular, P., Geuzaine, C., Henrotte, F., & Legros, W. (1998). A general environment for the treatment of discrete problems and its application to the finite element method. *IEEE transactions on magnetics*, *34*(5), 3395-3398.

Edwards, D., Cortes, M., Datta, A., Minhas, P., Wassermann, E. M., & Bikson, M. (2013). Physiological and modeling evidence for focal transcranial electrical brain stimulation in humans: a basis for high-definition tDCS. *Neuroimage*, *74*, 266-275.

Fernandes, S. R., Callejón-Leblic, M. A., & Ferreira, H. A. (2024). How does the electric field induced by tDCS influence motor-related connectivity? Model-guided perspectives. *Physics in Medicine & Biology*, *69*(5), 055007.

Gözenman, F., & Berryhill, M. E. (2016). Working memory capacity differentially influences responses to tDCS and HD-tDCS in a retro-cue task. *Neuroscience letters*, *629*, 105-109.

Helfrich, R. F., Knepper, H., Nolte, G., Strüber, D., Rach, S., Herrmann, C. S., ... & Engel, A. K. (2014). Selective modulation of interhemispheric functional connectivity by HD-tACS shapes perception. *PLoS biology*, *12*(12), e1002031.

Hogeveen, J., Grafman, J., Aboseria, M., David, A., Bikson, M., & Hauner, K. K. (2016). Effects of high-definition and conventional tDCS on response inhibition. *Brain stimulation*, *9*(5), 720-729.

Huang, Y., Liu, A. A., Lafon, B., Friedman, D., Dayan, M., Wang, X., ... & Parra, L. C. (2017). Measurements and models of electric fields in the in vivo human brain during transcranial electric stimulation. *elife*, *6*, e18834.

Huang, Y., Datta, A., Bikson, M., & Parra, L. C. (2019). Realistic volumetric-approach to simulate transcranial electric stimulation—ROAST—a fully automated open-source pipeline. *Journal of neural engineering*, *16*(5), 056006.

Hunold, A., Haueisen, J., Nees, F., & Moliadze, V. (2023). Review of individualized current flow modeling studies for transcranial electrical stimulation. *Journal of Neuroscience Research*, *101*(4), 405-423.

Jackson, M. P., Rahman, A., Lafon, B., Kronberg, G., Ling, D., Parra, L. C., & Bikson, M. (2016). Animal models of transcranial direct current stimulation: methods and mechanisms. *Clinical Neurophysiology*, *127*(11), 3425-3454.

Kar, K., Duijnhouwer, J., & Krekelberg, B. (2017). Transcranial alternating current stimulation attenuates neuronal adaptation. *Journal of Neuroscience*, *37*(9), 2325-2335.

Lafon, B., Rahman, A., Bikson, M., & Parra, L. C. (2017). Direct current stimulation alters neuronal input/output function. *Brain stimulation*, *10*(1), 36-45.

Masina, F., Arcara, G., Galletti, E., Cinque, I., Gamberini, L., & Mapelli, D. (2021). Neurophysiological and behavioural effects of conventional and high definition tDCS. *Scientific reports*, *11*(1), 7659.

Michelson, N. J., Eles, J. R., Vazquez, A. L., Ludwig, K. A., & Kozai, T. D. (2019). Calcium activation of cortical neurons by continuous electrical stimulation: Frequency dependence, temporal fidelity, and activation density. *Journal of neuroscience research*, *97*(5), 620-638.

Mishima, T., Nagai, T., Yahagi, K., Akther, S., Oe, Y., Monai, H., ... & Hirase, H. (2019). Transcranial direct current stimulation (tDCS) induces adrenergic receptor-dependent microglial morphological changes in mice. *eneuro*, *6*(5).

Monai, H., Ohkura, M., Tanaka, M., Oe, Y., Konno, A., Hirai, H., ... & Hirase, H. (2016). Calcium imaging reveals glial involvement in transcranial direct current stimulation-induced plasticity in mouse brain. *Nature communications*, *7*(1), 11100.

Opitz, A., Falchier, A., Yan, C. G., Yeagle, E. M., Linn, G. S., Megevand, P., ... & Schroeder, C. E. (2016). Spatiotemporal structure of intracranial electric fields induced by transcranial electric stimulation in humans and nonhuman primates. *Scientific reports*, *6*(1), 31236.

Opitz, A., Falchier, A., Linn, G. S., Milham, M. P., & Schroeder, C. E. (2017). Limitations of ex vivo measurements for in vivo neuroscience. *Proceedings of the National Academy of Sciences*, *114*(20), 5243-5246.

Opitz, A., Yeagle, E., Thielscher, A., Schroeder, C., Mehta, A. D., & Milham, M. P. (2018). On the importance of precise electrode placement for targeted transcranial electric stimulation. *Neuroimage*, *181*, 560-567.

Ozen, S., Sirota, A., Belluscio, M. A., Anastassiou, C. A., Stark, E., Koch, C., & Buzsáki, G. (2010). Transcranial electric stimulation entrains cortical neuronal populations in rats. *Journal of Neuroscience*, *30*(34), 11476-11485.

Paxinos, G., & Franklin, K. B. (2019). *Paxinos and Franklin's the mouse brain in stereotaxic coordinates* (5th ed.). Academic press.

Preisig, B. C., & Hervais-Adelman, A. (2022). The predictive value of individual electric field modeling for transcranial alternating current stimulation induced brain modulation. *Frontiers in Cellular Neuroscience*, *16*, 818703.

Reinhart, R. M. (2017). Disruption and rescue of interareal theta phase coupling and adaptive behavior. *Proceedings of the National Academy of Sciences*, *114*(43), 11542-11547.

Reinhart, R. M., & Nguyen, J. A. (2019). Working memory revived in older adults by synchronizing rhythmic brain circuits. *Nature neuroscience*, *22*(5), 820-827.

Thielscher, A., Antunes, A., & Saturnino, G. B. (2015, August). Field modeling for transcranial magnetic stimulation: A useful tool to understand the physiological effects of TMS?. In *2015 37th annual international conference of the IEEE engineering in medicine and biology society (EMBC)* (pp. 222-225). IEEE.

Violante, I. R., Alania, K., Cassarà, A. M., Neufeld, E., Acerbo, E., Carron, R., ... & Grossman, N. (2023). Non-invasive temporal interference electrical stimulation of the human hippocampus. *Nature neuroscience*, *26*(11), 1994-2004.

Vöröslakos, M., Takeuchi, Y., Brinyiczki, K., Zombori, T., Oliva, A., Fernández-Ruiz, A., ... & Berényi, A. (2018). Direct effects of transcranial electric stimulation on brain circuits in rats and humans. *Nature communications*, *9*(1), 483.

Zanto, T. P., Jones, K. T., Ostrand, A. E., Hsu, W. Y., Campusano, R., & Gazzaley, A. (2021). Individual differences in neuroanatomy and neurophysiology predict effects of transcranial alternating current stimulation. *Brain stimulation*, *14*(5), 1317-1329.

Zhang, D. W., Moraidis, A., & Klingberg, T. (2022). Individually tuned theta HD-tACS improves spatial performance. *Brain Stimulation*, *15*(6), 1439-1447.